Analyzing PEC Scattering Structure Using an IE-FFT Algorithm

Seung Mo Seo[1], Chao-Fu Wang [2], and Jin-Fa Lee [1]
[1] Department of Electrical Engineering
The Ohio State University, Columbus, OH 43212, USA
lee.1863@osu.edu

[2] Temasek Laboratories,
National University of Singapore,
5 Sports Drive 2, Singapore 117508, Singapore.
cfwang@nus.edg.sg

***Abstract*—** In this paper a fast integral equation method, termed IE-FFT, is developed, analyzed and applied to the electromagnetic (EM) solution of scattering problems. The methodology is developed for the Method of Moments (MoM) solution of the Electric Field Integral Equation (EFIE) on electrically large Perfect Electric Conducting (PEC) structures. Similar to other Fast Fourier Transform (FFT) based algorithms, IE-FFT uses a Cartesian grid to drastically decrease memory storage and speed up the matrix-vector multiplication. The IE-FFT algorithm employs two discretizations, one for the unknown current on an unstructured triangular mesh and the other on a uniform Cartesian grid for interpolating the Green's function. The uniform interpolation of the Green's function allows the fast computation of well-separated MoM interaction terms with the aid of a global FFT. Nevertheless, the coupling between near-interaction terms should be adequately corrected. The major contribution of this paper lies on the Lagrangian interpolation of the Green's function. This not only allows simple and efficient algorithmic implementation, but also naturally suggests a rigorous error analysis of the algorithm. The efficiency of the method is based on the Toeplitz structure of the interpolated Green's function. Therefore, it is applicable on both asymptotically-smooth and oscillatory kernels arisen in static and wave propagation problems, respectively. Through numerical simulations of electromagnetic wave scattering from a PEC sphere, the complexity of the IE-FFT algorithm is found to scale as $O(N^{1.5})$ and $O(N^{1.5}logN)$ for memory and CPU time, respectively. Various numerical results verify the high accuracy and efficiency of the method.

***Index Terms*—** Methods of Moment, Numerical method, Fast Fourier Transform, Electromagnetic Scattering, and Integral Equation.

I. INTRODUCTION

The Method of Moments (MoM) solution of surface Integral Equations (IE) has been proven very successfully in analyzing electromagnetic radiation and scattering from arbitrarily shaped conducting objects. A conventional MoM process produces high-accuracy results for both near- and far-field quantities, but requires prohibitive $O(n^2)$ memory and fill-in CPU time. This paper introduces yet another approach on reducing the computational burden of MoM while maintaining an explicit error control of the method.

During the last decades a large number of methods have been proposed to reduce the computational complexity and memory requirement of IE based methods. Perhaps the most successful and popular is the Fast Multipole Method (FMM) and its multilevel implementation MLFMM [1] – [4]. Careful implementations of MLFMM achieve $O(N)$ and $O(NlogN)$ complexities for memory and matrix-vector-multiplication time [2]. Unfortunately, the strong reliance of multipole-based methods on kernel-specific mathematical apparatus makes the methods inadequate for general purpose kernel-independent solvers.

Unlike FMM, a number of recent developments have focused on less kernel-dependent fast integral

methods. Such methods are the IES3 [6], IE-QR [7], [8] and Adaptive Cross-Approximation (ACA) [9], [10] algorithms. These are "algebraic" methods, in the sense that they consider the IE matrix from a linear algebra point of view. The computational reduction is achieved by compressing, in a multilevel fashion, the rank-deficient sub-matrices of geometrically well-separated interactions.

Another class of fast IE methods, which directly relates to the proposed method, is the grid-based or FFT-based category. The well-known precorrected-FFT (p-FFT) [11], [12] and the Adaptive Integral Method (AIM) [13], [14] are among the most popular and well documented. Both p-FFT and AIM approaches are of $O\left(N^{1.5}\right)$ for storage and $O(N^{1.5}\log N)$ for matrix-vector multiplication. Both approaches are based on an "equivalent" source approximation. Namely, the unstructured grid sources are mapped onto a uniformly distributed set of equivalent multipole moment sources. To establish "equivalence", the fields of the two sets of sources need to be matched at selected locations. Recently, a fast, high-order algorithm, based on "two-face" equivalent source approximation, was proposed in [15]. The fast, high-order algorithm achieves $O\left(N^{6/5}\log N\right)$ to $O\left(N^{4/3}\log N\right)$ by placing equivalent sources only on the faces of cubic cells. Nevertheless, the method is strongly dependent of the integral kernel due to the use of the addition theorem. The Sparse-Matrix/Canonical-Grid (SM/CG) method of [16] is yet another grid-based fast IE method. Unlike previous mentioned methods, The SM/CG method does not utilize equivalent sources, but employs the Taylor expansion of the Green's functions on a uniformly spaced canonical grid. Subsequently, the impedance matrix is solved by an FFT-based iterative procedure based on the number of Taylor expansion terms. The SM/CG method does require the detail knowledge of the integral kernel. Due to the Toeplitz symmetry, the memory complexity of SM/CG is $O\left(N^{1.5}\right)$. Gedney in [17] proposed the Quadrature Sampled Pre-Corrected Fast-Fourier Transform (QS-PCFFT) algorithm to project the unknown currents to a uniform grid. The QS-PCFFT algorithm evaluates the discrete Fourier transform of the current directly using discontinuous FFT, which is based on quadrature sampling of the currents. The algorithm provides controllable accuracy and exponential convergence. Finally, the Green's function interpolation together with the FFT (GIFFT) [18] algorithm has developed for arrays with arbitrary shape. The GIFFT algorithm uses an array mask function to identify the array boundaries and specify the domain on which the Green's function is interpolated. The FFT is used to accelerate the matrix-vector products in an iterative solver. Consequently, the GIFFT algorithm reduces storage and solution time. For volume IE methods and planar structures, all grid or FFT-based algorithms end up with $O(N)$ complexity for the memory.

The IE-FFT algorithm described in this paper is in essence the same as the GIFFT algorithm, although developed completely independent. Its basic attributes can be summarized in its simplicity, error control and generality due to the Lagrangian interpolation of the kernel, and efficiency due to the FFT. Before start summarizing the approach, it should be emphasized that the choice of Lagrange interpolation of the Green's function was based on the simplicity. Only minor modifications are needed to extend to other standard interpolation schemes such as Hierarchical Lagrangian, Newton, trigonometric, etc. The proposed approach is more versatile than the FMM and is also simpler than other grid-based methods. The less-kernel dependent algorithm is easily applied to various applications with little modification. For fast evaluation of integral operators, simple polynomial interpolation of the integral kernel is constructed on a regular grid. The IE-FFT algorithm employs algebraically simple Lagrange polynomials on each 3-D Cartesian cell. Regardless of the order of the polynomials and the electrical size of the scatterer, the sampling segments per wavelength should be kept constant. In accordance to the Nyquist sampling theorem, the proposed algorithm for 3-D surface IE leads to $O\left(N^{1.5}\right)$ complexity for the memory requirement. Unlike p-FFT and AIM methods, uniform grid does not represent "equivalent" source, but correspond to interpolation tools for the Green's functions. The error analysis of IE-FFT algorithm is considerably easier than other grid-based

methods due to Lagrangian interpolations. Upper bounds of the Green's function interpolation error versus the sampling segments are derived and verified for arbitrary polynomial orders. High order polynomials or more sampling segments for the interpolation could be chosen to get improved accuracy. The trade-off could be straightforwardly controlled over the accuracy and efficiency of the IE-FFT algorithm. Finally, the IE-FFT algorithm demonstrates $O\left(N^{1.5}\right)$ complexity and achieves good accuracy for solving 3-D arbitrarily shaped PEC scattering structures. Since the proposed method shares many common features with other FFT based methods, it is expected to achieve almost linear complexity when used to accelerate planar (2.5D) multilayer IE solvers or volume integral equations (VIEs).

The outline of the paper is as follows. For completeness a short summary of the EFIE formulation for 3-D PEC scattering problems is described in Section II. The algorithmic development and details of the IE-FFT algorithm are presented in Section III. Section IV is devoted to the error analysis of the algorithm, and to demonstrate the error control of interpolating the Green's function. To validate the theory and analytical developments, scattering from a PEC sphere is first considered in Section V. Through numerous numerical experiments, the accuracy and performance of the current approach are demonstrated. Finally, the proposed method is tested, and compared with other methods, in an example involving the scattering from a generic battleship. Concluding remarks are discussed in Section VI.

II. FORMULATION

Let's start with the discrete Galerkin statement for the electric field integral equation (EFIE), find $\vec{J}_h\left(\vec{r}\right) \in \mathbf{X}_h \subset \mathbf{H}_{\|}^{-1/2}\left(\mathbf{div}_\Gamma;\Gamma\right)$ such that

$$k_0^2 \int_{\Gamma_h} \vec{\lambda}_h\left(\vec{r}\right) \cdot \int_{\Gamma_h} g\left(\vec{r};\vec{r}'\right) \vec{J}_h\left(\vec{r}'\right) dx'^2 dx^2 - \int_{\Gamma_h} \mathbf{div}_\Gamma \vec{\lambda}_h\left(\vec{r}\right) \int_{\Gamma_h} g\left(\vec{r};\vec{r}'\right) \mathbf{div}'_\Gamma \vec{J}_h\left(\vec{r}'\right) dx'^2 dx^2 = -\frac{jk_0}{\eta_0} \int_{\Gamma_h} \vec{\lambda}_h\left(\vec{r}\right) \cdot \vec{E}^{inc}\left(\vec{r}\right) dx^2 \quad , \forall \vec{\lambda}_h \in \mathbf{X}_h , \quad (1)$$

where Γ_h denotes the facetized surface of the PEC object. $\mathbf{X}_h$ is the finite dimensional trial and testing spaces, and $\mathbf{H}_{\|}^{-1/2}\left(\mathbf{div}_\Gamma;\Gamma\right) = \left\{ \vec{v} \,\middle|\, \vec{v} \in \left(L^2\left(\Gamma\right)\right)^2, \quad \mathbf{div}_\Gamma \vec{v} \in L^2\left(\Gamma\right) \right\}$ is the correct spaces where the unknown currents reside [20]. The unknown electric current density is denoted by $\vec{J}_h\left(\vec{r}\right)$ and the testing function is $\vec{\lambda}\left(\vec{r}\right)$. $\vec{r}$ and $\vec{r}'$ are observation and source points, respectively, and $\vec{E}^{inc}\left(\vec{r}\right)$ is the incident electric field. In the present application, the free-space Green's function $g\left(\vec{r};\vec{r}'\right)$ is considered. The free space wave number and characteristic impedance are respectively denoted by k_0 and η_0. Throughout the paper the $e^{j\omega t}$ time convention is assumed, and j denotes the imaginary unit, except when stated otherwise. From the discrete Galerkin statement a system of equations is obtained by expanding trial and testing functions into a set of basis functions

$$\vec{J}_h\left(\vec{r}'\right) = \sum_{i=0}^{N-1} J_i \vec{\alpha}_i\left(\vec{r}'\right), \quad (2)$$

where $\vec{\alpha}\left(\vec{r}\right)'s$ are surface div-conforming vector Rao-Wilton-Glisson (RWG) basis functions [19]. Finally, the resulting matrix equation can be written as

$$\mathbf{Z} \bullet \mathbf{J} = \mathbf{V} . \quad (3)$$

The entries of the impedance matrix $\mathbf{Z}$ and those of the right-hand vector $\mathbf{V}$ are given by

$$Z_{ij} = k_0^2 A_{ij} - D_{ij}, \quad 0 \le i, j \le N-1, \quad (4)$$

where

$$A_{ij} = \int_{\mathrm{supp}(\vec{\alpha}_i)} \vec{\alpha}_i\left(\vec{r}\right) \cdot \int_{\mathrm{supp}(\vec{\alpha}_j)} g\left(\vec{r};\vec{r}'\right) \vec{\alpha}_j\left(\vec{r}'\right) dx'^2 dx^2$$
$$D_{ij} = \int_{\mathrm{supp}(\vec{\alpha}_i)} \mathbf{div}_\Gamma \vec{\alpha}_i\left(\vec{r}\right) \int_{\mathrm{supp}(\vec{\alpha}_j)} g\left(\vec{r};\vec{r}'\right) \mathbf{div}'_\Gamma \vec{\alpha}_j\left(\vec{r}'\right) dx'^2 dx^2 \quad (5)$$

and

$$V_i = -\frac{jk_0}{\eta_0} \int_{\mathrm{supp}(\vec{\alpha}_j)} \vec{\alpha}_i\left(\vec{r}\right) \cdot \vec{E}^{inc}\left(\vec{r}\right) dx^2 , \quad (6)$$

where N is the number of unknowns, notice that *supp()* indicates the finite support of every non-boundary edge related basis function.

III. IE-FFT ALGORITHM

As stated in the introduction, the heart of the IE-FFT algorithm is the uniform Cartesian interpolation of the Green's function. The IE-FFT algorithm starts by constructing a rectangular bounding box that encloses the entire

computational domain. This box is the domain for interpolating the Green's functions. The key outcome of the Green's functions interpolation is the decoupling of the sources and the receivers. This is the same idea as the FMM, but instead of approximation the Green's function through the spherical multipole expansion, the Green's function is expanded into a Cartesian Lagrange polynomial. Therefore the Green's function can be expressed as

$$g(\vec{r};\vec{r}') = \frac{e^{-jk_0|\vec{r}-\vec{r}'|}}{|\vec{r}-\vec{r}'|} \simeq \sum_{n=0}^{N_g-1}\sum_{n'=0}^{N_g-1} \beta_n^p(\vec{r})\, g_{n,n'} \beta_{n'}^p(\vec{r}'), \quad (7)$$

where p is the order of Lagrange polynomial interpolation, N_g is the number of grid points, β_n^p and $\beta_{n'}^p$ are the p^{th} order Lagrange interpolation basis functions for grids $\vec{r}$ and $\vec{r}'$, $g_{n,n'}$ are the Lagrange coefficients of the Green's function, and n and n' are dimensional indexes of grids $\vec{r}$ and $\vec{r}'$, respectively The explicit forms of β_n^p can be found in a number of elementary interpolation books such as [21]. In equation (7), the source and observation terms for the Lagrange interpolation basis functions are completely decoupled. Having obtained the product form of $g(\vec{r};\vec{r}')$ the coupling integrals of (5) are now written as

$$A_{ij} \simeq \int_{\mathrm{supp}(\vec{\alpha}_i)} \vec{\alpha}_i(\vec{r}) \cdot \int_{\mathrm{supp}(\vec{\alpha}_j)} \left[\sum_{n=0}^{N_g-1}\sum_{n'=0}^{N_g-1} \beta_n^p(\vec{r})\, g_{n,n'} \beta_{n'}^p(\vec{r}')\right] \vec{\alpha}_j(\vec{r}')\, dx'^2\, dx^2, \quad (8)$$

and

$$D_{ij} \simeq \int_{\mathrm{supp}(\vec{\alpha}_i)} \mathbf{div}_\Gamma \vec{\alpha}_i(\vec{r}) \cdot \left(\int_{\mathrm{supp}(\vec{\alpha}_j)} \left[\sum_{(n)=0}^{N_g-1}\sum_{(n')=0}^{N_g-1} \beta_n^p(\vec{r})\, g_{n,n'} \beta_{n'}^p(\vec{r}')\right] \mathbf{div}'_\Gamma \vec{\alpha}_j(\vec{r}')\, dx'^2 \right) dx^2, \quad (9)$$

respectively. Interchanging summation and integration orders, and grouping primed and unprimed variables, leads to

$$A_{ij} \simeq \sum_{n=0}^{N_g-1}\sum_{n'=0}^{N_g-1} \int_{\mathrm{supp}(\vec{\alpha}_i)} \left\{ \left(\vec{\alpha}_i(\vec{r})\beta_n^p(\vec{r})\right) g_{n,n'} \cdot \int_{\mathrm{supp}(\vec{\alpha}_j)} \left(\beta_{n'}^p(\vec{r}')\vec{\alpha}_j(\vec{r}')\right) dx'^2 \right\} dx^2, \quad (10)$$

and

$$D_{ij} \simeq \sum_{n=0}^{N_g-1}\sum_{n'=0}^{N_g-1} \int_{\mathrm{supp}(\vec{\alpha}_i)} \left\{ \left(\mathbf{div}_\Gamma \vec{\alpha}_i(\vec{r})\beta_n^p(\vec{r})\right) g_{n,n'} \cdot \int_{\mathrm{supp}(\vec{\alpha}_j)} \left(\beta_{n'}^p(\vec{r}')\mathbf{div}'_\Gamma \vec{\alpha}_j(\vec{r}')\right) dx'^2 \right\} dx^2. \quad (11)$$

The product forms of impedance matrix terms in (10)(11) are valid for all interactions, except the ones that reside on the same Green's function cell. At these location the Green's function coefficient matrix $g_{n,n'}$ is singular, thus need to be appropriately corrected. In summary the IE-FFT algorithm proceeds in four steps:

1) Represent free-space Green's function as simple Lagrange polynomials.
2) Construct four projection matrices **Π** using the EFIE formulation.
3) Correct entries from near-interaction elements.
4) Accelerate the matrix-vector products using the global FFT.

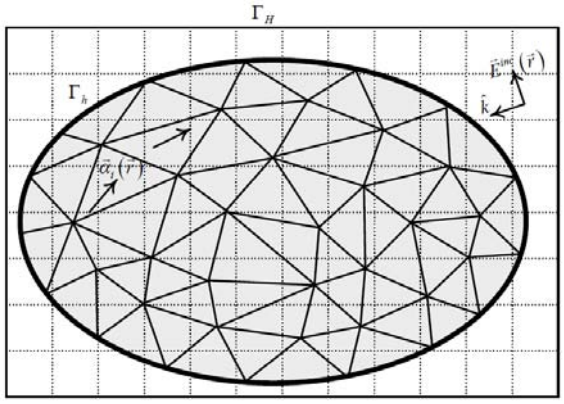

Fig. 1. Two discretizations for a problem domain. One is the regular triangular mesh (inside the boundary Γ_h on the scatterer) for the unknown surface current induced by the incident field. The other is a uniform Cartesian grid of the rectangular box (Γ_H) enclosing the problem domain.

The detail of the IE-FFT algorithm could be shown below.

A. Representation of Green's function using simple Lagrange polynomials

To interpolate the 3-D free-space Green's function, a rectangular box with dimension $L_x \times L_y \times L_z$ in the Cartesian coordinate is constructed first. The rectangular bounding box that encloses the problem domain, as shown in Fig. 1, will be considered as the domain of the Green's function. The bounding box is uniformly interpolated with simple Lagrange polynomials. In the current implementation, the sampling segment between two grid points is typically set to

be $d = \lambda / 7$. The number of sampling points affects the accuracy of the approximation, and need to exceed Nyquist sampling rate for good accuracy. In equation (7), the number of grid points is $N_g = N_x \times N_y \times N_z$ where $N_x = L_x / d$, $N_y = L_y / d$, and $N_z = L_z / d$. Also, the dimensional indexes could be expressed as $n = (i, j, k)$ and $n' = (i', j', k')$ where $0 \le i, i' < N_x$, $0 \le j, j' < N_y$, and $0 \le k, k' < N_z$. The p^{th} order interpolation basis functions β_n^p are the 3-D tensor products form of one-dimensional piecewise Lagrange polynomials on a Cartesian grid

$$\beta_n^p(\vec{r}) = \beta_i^p(x) \cdot \beta_i^p(y) \cdot \beta_k^p(z). \quad (12)$$

Combined with equation (7) and(12), the Green function is written in the matrix form

$$g(\vec{r};\vec{r}') \simeq \left(\boldsymbol{\beta}(\vec{r})\right)^T \bullet \mathbf{G} \bullet \boldsymbol{\beta}(\vec{r}'), \quad (13)$$

where

$$\boldsymbol{\beta}(\vec{r}) = \left[\beta_0^p(\vec{r}) \quad \beta_1^p(\vec{r}) \quad \cdots \quad \beta_{N_g-1}^p(\vec{r})\right] = \begin{bmatrix} \beta_0^p(x)\beta_0^p(y)\beta_0^p(z) \\ \beta_1^p(x)\beta_0^p(y)\beta_0^p(z) \\ \vdots \\ \beta_{N_x-1}^p(x)\beta_{N_y-1}^p(y)\beta_{N_z-1}^p(z) \end{bmatrix}^T, \quad (14)$$

$$\mathbf{G} = \begin{bmatrix} g_{0,0} & g_{0,1} & \cdots & g_{0,N_g} \\ g_{1,0} & g_{1,1} & \cdots & g_{1,N_g} \\ \vdots & \vdots & \ddots & \vdots \\ g_{N_g,0} & g_{N_g,1} & \cdots & g_{N_g,N_g} \end{bmatrix}. \quad (15)$$

For general Green's function, one needs to store the entire $\mathbf{G}$, resulting in a $O\left(N_g^2\right)$ storage. Fortunately, most of the Green's functions appearing in static or electromagnetic field computations are of a difference-form. Namely, $g(\vec{r};\vec{r}') = g(\vec{r} - \vec{r}')$. Naturally, such integral kernels would lead to a 3-D block-Toeplitz structure for equation . For a 3-D block-Toeplitz matrix, we only need to store $2N_g$ entries of the $\mathbf{G}$. As it was mentioned above, the numerical values of $g_{n-n'}$ for $n = n'$ are infinite. For simplicity, they are set to zero, and the near field contributions will be appropriately corrected during the correction step.

B. Representation of Π matrices

There are two projection matrices needed in the IE-FFT algorithm, as evidenced from equation (10) and (11). They are:

$$\vec{\boldsymbol{\Pi}}_A = \int_\Gamma \begin{bmatrix} \vec{\alpha}_0(\vec{r}) \\ \vec{\alpha}_1(\vec{r}) \\ \vdots \\ \vec{\alpha}_{N-1}(\vec{r}) \end{bmatrix} \left[\beta_0^p(\vec{r}) \quad \beta_1^p(\vec{r}) \quad \cdots \quad \beta_{N_g-1}^p(\vec{r})\right] dx^2 , \quad (16)$$

and

$$\boldsymbol{\Pi}_D = \int_\Gamma \begin{bmatrix} \mathbf{div}_\Gamma \vec{\alpha}_0(\vec{r}) \\ \mathbf{div}_\Gamma \vec{\alpha}_1(\vec{r}) \\ \vdots \\ \mathbf{div}_\Gamma \vec{\alpha}_{N-1}(\vec{r}) \end{bmatrix} \left[\beta_0^p(\vec{r}) \quad \beta_1^p(\vec{r}) \quad \cdots \quad \beta_{N_g-1}^p(\vec{r})\right] dx^2 \quad (17)$$

respectively. Notice that $\vec{\boldsymbol{\Pi}}_A$ is a vector-valued matrix. Both matrices (16) and (17) are non-symmetric and more importantly sparse, since both RWG and the Lagrange interpolation basis functions have finite support. In other words, each RWG basis function is just projected onto only a few Lagrangian cells. Therefore, the memory requirement and CPU time of computing these matrices are $O(N)$.

C. Correction of matrix entries for touching or overlapping cells

From equation (5), the accuracy of approximating Z_{ij} by the IE-FFT algorithm depends on the distance between i^{th} basis and j^{th} testing functions. These functions are separated at least by $\alpha\lambda$ (we chose $\alpha = 0.2$) to assure accuracy in Fig. 2. In other words, the coupling between near-interaction terms should be adequately corrected. These entries should be substituted by accurate ones, which are computed by the conventional MoM technique. These entries should be corrected for fast computation before the matrix-vector products are performed. Finally, the correction entries from the interaction between i^{th} and j^{th} RWG basis functions are written as

$$Z_{ij}^{corr} = Z_{ij}^{MoM} - k_0^2 \left(\vec{\Pi}_A\right)_{iI} G_{IJ} \left(\vec{\Pi}_A\right)_{Jj}^T + \left(\Pi_D\right)_{iI} G_{IJ} \left(\Pi_D\right)_{Jj}^T , \quad (18)$$

where $0 \le i < N$, $j \in C_{neig}$, and C_{neig} is the set of the near-interaction elements. The coupling between basis function i and j will be corrected by (18) if they are separated less than 0.2λ (our choice). The correction matrix $\mathbf{Z}^{corr}$ is unquestionably sparse. In the current implementation, the memory of correction matrix does not depends on the sampling segment of Cartesian grid and the order of Lagrange

interpolation basis functions, used to interpolate the Green's function.

D. Fast matrix vector multiplication

Let Z_{ij} represent one entry of the impedance matrix and the matrix-vector product is written as

$$y_i = \sum_{j=0}^{N-1} Z_{ij} x_j , \quad 0 \le i < N-1 . \tag{19}$$

Combined with IE-FFT algorithm, the matrix-vector products could be rewritten as

$$\begin{aligned} y &= Z^{corr} \cdot x \\ &+ k_0^2 \vec{\Pi}_A \cdot IFFT\left\{ FFT(G) \cdot FFT\left(\left(\vec{\Pi}_A\right)^T \cdot x \right) \right\} \cdot \\ &- \Pi_D \cdot IFFT\left\{ FFT(G) \cdot FFT\left(\left(\Pi_D\right)^T \cdot x \right) \right\} \end{aligned} \tag{20}$$

From the above expression, the significant saving of memory due to the $O(N)$ complexity of $\mathbf{Z}^{corr}$ and $\mathbf{\Pi}$ matrices is clearly shown. Note that the FFT of the $\mathbf{G}$ matrix is computed only once. The memory requirement of the coefficient is $O\left(N^{1.5}\right)$ complexity. However, the FFT can be applied to speed up matrix vector multiplications significantly. It leads to $O\left(N^{1.5}\log N\right)$ complexity.

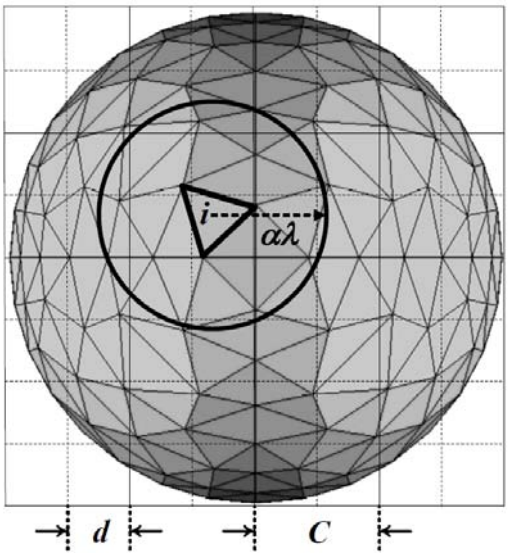

Fig. 2 A PEC sphere with two discretizations, a triangular mesh and a uniform Cartesian grid. Note that in the figure, *d* is the sampling resolution, *C* is the size of the Cartesian element, α is a constant used to define the local correction region, and λ is the wavelength.

IV. ERROR CONTROL

The only additional approximation of IE-FFT algorithm compared to the conventional MoM comes from the interpolation of the Green's function. Consequently, in order to assess the accuracy of the IE-FFT algorithm alone, the error analysis of the Green's function interpolation need to be considered. This section provides an error bound, which will guide the practical implementation of the IE-FFT algorithm for 3-D PEC scattering problems.

A. p^{th} order interpolation

Consider an analytical function $f(x),\ a \le x \le b$. A unique p^{th} order interpolation $f^{[p]}(x),\ a \le x \le b$ can be determined with

$$f^{[p]}(x_i) = f(x_i), a \le x_i \le b \quad x = 0, \cdots, p \tag{21}$$

Moreover, by Cauchy reminder theorem [21] for polynomial interpolation, we have

$$\begin{aligned} &\forall x \in [a,b], \exists \xi \in [a,b], s.t. \\ &f(x) - f^{[p]}(x) \\ &\quad = \frac{(x-x_0)(x-x_1)\cdots(x-x_p)}{(p+1)!} f^{(p+1)}(\xi), \end{aligned} \tag{22}$$

where $f^{(p+1)}(x)$ denotes the $(p+1)$ derivative of $f(x)$ at x. Subsequently, the following error bound is valid

$$\begin{aligned} &\frac{\left| f(x) - f^{[p]}(x) \right|}{\left| f(x) \right|} \le \\ &\qquad \frac{\max\limits_{a \le x \le b} \prod\limits_{i=0}^{p} \left| x - x_i \right|}{\left| f(x) \right|} \cdot \frac{\max\limits_{a \le \xi \le b} \left| f^{(p+1)}(\xi) \right|}{(p+1)!} \end{aligned} . \tag{23}$$

B. Free space Green's function and its derivatives

For free space scattering applications, $f(x) = \frac{\left(e^{-jk_0 x}\right)}{x}$ is considered. Note here that in order to fulfill the assumption that $f(x)$ is to be analytic, separation by $\alpha\lambda$ to be called well-separated should be persevered. The derivatives of $f(x)$ are summarized below

$$
\begin{aligned}
f(x) &= \frac{e^{-jk_0x}}{x} \\
f^{(1)}(x) &= -\left(jk_0+\frac{1}{x}\right)\frac{e^{-jk_0x}}{x} \\
f^{(2)}(x) &= \left(jk_0+\frac{1}{x}\right)^2\frac{e^{-jk_0x}}{x}+\frac{1}{x^2}\frac{e^{-jk_0x}}{x} \\
f^{(3)}(x) &= -\left(jk_0+\frac{1}{x}\right)^3\frac{e^{-jk_0x}}{x}-\left(jk_0+\frac{1}{x}\right)\frac{3}{x^2}\frac{e^{-jk_0x}}{x} \\
&\quad -\frac{2}{x^3}\frac{e^{-jk_0x}}{x} \\
f^{(4)}(x) &= \left(jk_0+\frac{1}{x}\right)^4\frac{e^{-jk_0x}}{x}+\left(jk_0+\frac{1}{x}\right)^2\frac{3}{x^2}\frac{e^{-jk_0x}}{x} \\
&\quad +\left(jk_0+\frac{1}{x}\right)\left(jk_0+\frac{3}{x}\right)\frac{3}{x^2}\frac{e^{-jk_0x}}{x} \\
&\quad +\left(jk_0+\frac{4}{x}\right)\frac{2}{x^3}\frac{e^{-jk_0x}}{x}+\frac{3}{x^4}\frac{e^{-jk_0x}}{x} \\
&\quad \vdots
\end{aligned}
\tag{24}
$$

C. Upper error bound in the IE-FFT algorithm

For p^{th} order interpolation polynomial in the IE-FFT algorithm, $b=a+pd$ and $d=\lambda/n$ are given (where n is the number of segments per wavelength). Also, as mentioned earlier, to assure the analyticity of the integral kernel, $a \geq \alpha\lambda$ should be kept. Furthermore, in the current IE-FFT implementation, uniform sampling is simply adopted, namely $|x_{i+1}-x_i|=d$. Subsequently, the following equation holds

$$
\frac{\max\limits_{a\le x\le b}\prod\limits_{i=0}^{p}|x-x_i|}{|f(x)|} \le \begin{cases} \dfrac{2}{3\sqrt{3}}\left[\alpha+\dfrac{0.42}{n}\right]d^3, & p=2 \\ \left[\alpha+\dfrac{0.38}{n}\right]d^4, & p=3 \\ \vdots & \vdots \end{cases} \tag{25}
$$

Additionally, we have the following inequalities

$$
\max_{a\le\xi\le b}\frac{\left|f^{(p+1)}(p)\right|}{(p+1)!} \le \begin{cases} \dfrac{1}{a}\left[\sigma_1^3+\dfrac{3\sigma_1}{a^2}+\dfrac{2}{a^3}\right]\dfrac{1}{3!}, & p=2 \\ \dfrac{1}{a}\left[\sigma_1^4+\dfrac{3\sigma_1^2}{a^2}+\dfrac{3\sigma_1\sigma_3}{a^2}+\dfrac{2\sigma_4}{a^3}+\dfrac{3}{a^4}\right]\dfrac{1}{4!}, & p=3 \\ \vdots & \vdots \end{cases} \tag{26}
$$

In equation (26), the parameters σ_i are given by

$$
\begin{aligned}
\sigma_1 &= \sqrt{k_0^2+\left(\frac{1}{a}\right)^2} \le k_0\sqrt{1+\left(\frac{1}{2\pi\alpha}\right)} \\
\sigma_3 &= \sqrt{k_0^2+\left(\frac{3}{a}\right)^2} \le k_0\sqrt{1+\left(\frac{3}{2\pi\alpha}\right)} \\
\sigma_4 &= \sqrt{k_0^2+\left(\frac{4}{a}\right)^2} \le k_0\sqrt{1+\left(\frac{2}{\pi\alpha}\right)}
\end{aligned}
\tag{27}
$$

Substituting equation (24), (25) and (26) into (23) results in the final upper bound for the IE-FFT algorithm in (28) below.

In summary, the upper error bounds for the relative interpolation error versus the sampling segments, n, is plotted in Fig. 3 with $\alpha=0.2$. The resulting equation is given by (29).

$$
\frac{\left|f(x)-f^{[p]}(x)\right|}{|f(x)|} \le \begin{cases} \dfrac{88}{n^3}\left[1+\dfrac{2.1}{n}\right], & p=2 \\ \dfrac{172}{n^4}\left[1+\dfrac{1.9}{n}\right], & p=3 \\ \vdots & \vdots \end{cases} \tag{29}
$$

The second-order and third-order interpolation polynomials in the IE-FFT are plotted with squares and circles. Fig. 4 shows the upper error bound for the relative interpolation error versus the minimum distance, α with $n=7$. We should point out that in Fig. 4, the error approaching a constant as $\alpha\to\infty$. This is the unique feature of the wave propagation problems. Namely, any high-order derivatives

$$
\frac{\left|f(x)-f^{[p]}(x)\right|}{|f(x)|} \le \begin{cases} 16\left[\left(\dfrac{\sigma_1}{k_0}\right)^3+\left(\dfrac{\sigma_1}{k_0}\right)\dfrac{3}{(2\pi\alpha)^2}+\dfrac{2}{(2\pi\alpha)^3}\right]\left[1+\dfrac{0.42}{\alpha n}\right]\dfrac{1}{n^3}, & p=2 \\ 10\left[\left(\dfrac{\sigma_1}{k_0}\right)^4+\left(\dfrac{\sigma_1}{k_0}\right)^2\dfrac{3}{(2\pi\alpha)^2}+\left(\dfrac{\sigma_1\sigma_3}{k_0^2}\right)\dfrac{3}{(2\pi\alpha)^2}+\left(\dfrac{\sigma_4}{k_0}\right)\dfrac{2}{(2\pi\alpha)^3}+\dfrac{3}{(2\pi\alpha)^4}\right]\left[1+\dfrac{0.38}{\alpha n}\right]\dfrac{1}{n^4}, & p=3 \\ \vdots & \vdots \end{cases} \tag{28}
$$

of the Green's function will always exhibit $O(1/x)$ behavior asymptotically. If this is for static applications, the error will approach zero as $\alpha \to \infty$.

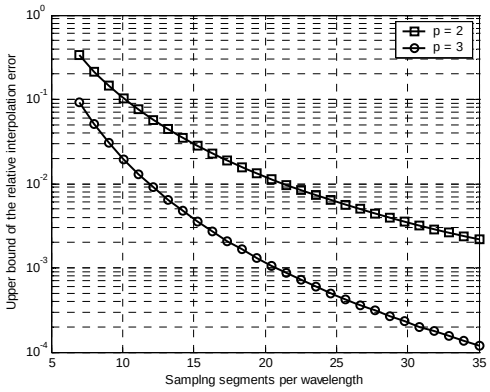

Fig. 3 Error bounds of the interpolated Green's function, plotted as a function of sampling rate and with p=2 and p=3.

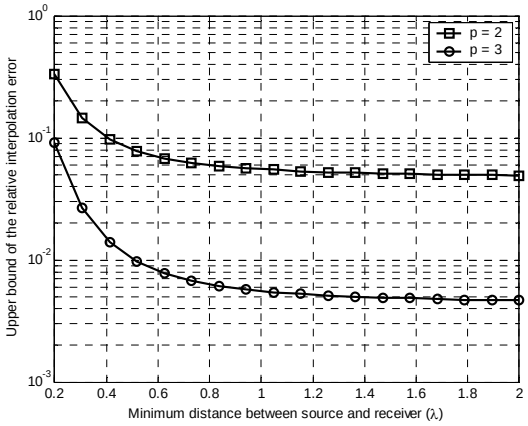

Fig. 4 Plots of upper error bounds for the Green's function interpolation of the IE-FFT algorithm as a function of minimum distance between source and receiver.

V. NUMERICAL RESULTS

In this section, studies on two numerical examples are conducted in order to demonstrate the complexity and accuracy of the IE-FFT algorithm. The EM scattering from a PEC sphere of various electrical sizes is first computed to validate the accuracy and efficiency of the IE-FFT algorithm. To demonstrate the IE-FFT algorithm, second-order and third-order Lagrange polynomials for interpolating the Green's function are used. For a very large-scale realistic problem, the scattering of a generic battleship, is considered. All numerical experiments are carried out on a 16 GB RAM, AMD® Opteron™ 246 64-bit workstation. All computations in this section have been performed in single precision arithmetic.

A. A PEC sphere

Scattering from a PEC sphere of radius 1 meter is first considered to demonstrate the complexity of the IE-FFT algorithm. In this example, the mesh density is kept constant, e.g. $h = \lambda/7$, while the operating frequency increases. Table 1 and Table 2 summarize the performance, in terms of memory, of the IE-FFT algorithm for second-order and third order Lagrange polynomials, respectively. The total memory is split into the last three columns of each table, representing each individual matrix involved in (18).

Table 1: Memory requirement of the IE-FFT algorithm ($p = 2$) for scattering from a perfect conducting sphere

Frequency (MHz)	Unknowns	$\mathbf{Z}^{corr}$ (MB)	$\vec{\Pi}_A + \Pi_D$ (MB)	$\mathbf{G}$ (MB)
600	12,288	7.0	7.6	3.1
1,200	49,152	28.1	30.7	24.4
2,400	196,608	112.7	124.8	194.6
4,800	786,432	450.8	502.4	1547.7

Table 2: Memory requirement of the IE-FFT algorithm ($p = 3$) for scattering from a perfect conducting sphere

Frequency (MHz)	Unknowns	$\mathbf{Z}^{corr}$ (MB)	$\vec{\Pi}_A + \Pi_D$ (MB)	$\mathbf{G}$ (MB)
600	12,288	7.0	17.1	3.1
1,200	49,152	28.1	67.7	24.4
2,400	196,608	112.7	274.0	194.6
4,800	786,432	450.8	1088.7	1547.7

Having addressed the complexity of the algorithm, we shall now address the accuracy. For that reason, the bistatic echo area or scattering cross section (SCS) results of the IE-FFT algorithm for $p = 2$ are compared with those of the conventional MoM and Mie series solution in Fig. 5(a). To further quantify the error, the RMS error of the SCS is reported in each figure. The RMS error of SCS calculation is defined as

$$\eta = \sqrt{\frac{\int_0^{2\pi}\int_0^{\pi} \left| SCS_{IE-FFT}(\theta,\phi) - SCS_{Mie}(\theta,\phi) \right|^2 \sin\theta d\theta d\phi}{\int_0^{2\pi}\int_0^{\pi} \left| SCS_{Mie}(\theta,\phi) \right|^2 \sin\theta d\theta d\phi}} \quad (30)$$

where θ and ϕ are angles of the observation points, $SCS_{Mie}(\theta,\phi)$ is the SCS calculation by the Mie series, and $SCS_{IE-FFT}(\theta,\phi)$ is that of the IE-FFT algorithm. For MoM, the RMS error of SCS calculation relative to Mie series is computed as 6.2727e-04. The bistatic SCS solutions of MoM are very well matched to those of Mie series. For IE-FFT algorithm, the RMS error relative to MoM solutions is also computed and corresponds to 0.0443. The bistatic SCS is in very good agreement with that of MoM. The accuracy can be improved by increasing the order of the Lagrange polynomials or the sampling segments per wavelength, in the interpolation of the Green's function. Fig. 5(b) shows the improvement of the bistatic SCS calculations. By increasing the order of the Lagrange polynomials or the sampling segments, each RMS error has improved to 0.0165 and 0.0074, respectively. For the second-order and third-order Lagrange polynomials, 11 and 7 sampling segments per wavelength are used, respectively. To summarize these experiments, the RMS errors versus the size of sampling segments per wavelength are plotted in Fig. 6 for second-order and third order interpolation. Figure 7 compares the bistatic SCS from the IE-FFT algorithm ($p = 2,3$) with the result from Mie series at 2.4 GHz. It corresponds to 196,608 unknowns. The electrical size of the PEC sphere is 16λ . The memory of MoM and **II** matrices, and the coefficients of Green's function are about 432 MB for second-order interpolation, and 661 MB for third-order interpolation. Both results agree very well with the solution of Mie series. As expected, the result from the third-order polynomials is more accurate. The RMS error of SCS is computed to be 0.0494 and 0.0160, respectively. In Fig.8, the bistatic SCS of the sphere with diameter 32λ is plotted. The number of IE-FFT unknowns is 786,432. The result of IE-FFT algorithm agrees well with those of Mie series. However, $p = 2$ answer oscillates around the exact values. The solution is improved by increasing the order of the polynomials, not by increasing the sampling segments. Due to $O(N^{1.5})$ complexity, increasing the order of the polynomials is preferred in electrically large problems. The total memory required is about 2.5 and 3.1 GB for second and third order polynomials, respectively.

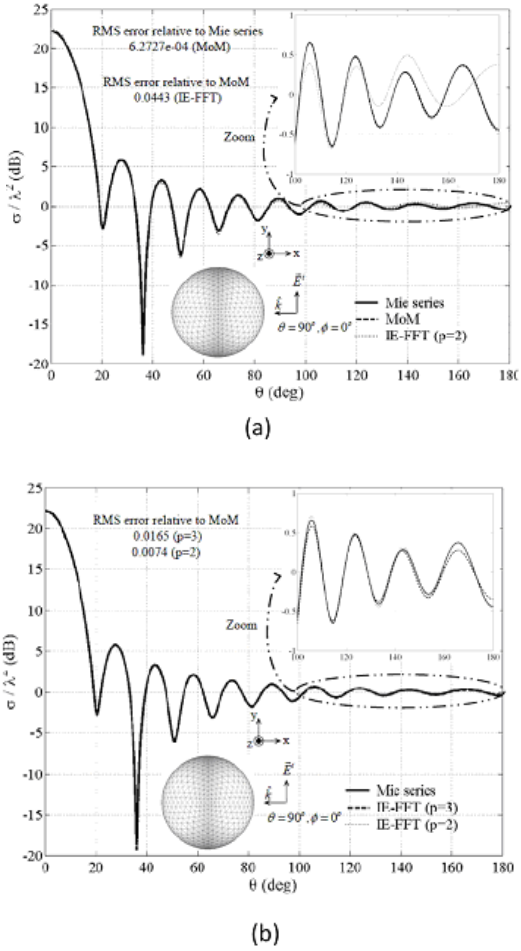

Fig. 5 Bistatic SCS for a PEC 4λ sphere. (a) IEFFT results, using p = 2 (d=λ/7); (b) using p = 2 (d=λ/7) and p = 3 (d=λ/7) with comparisons to conventional MoM and Mie series.

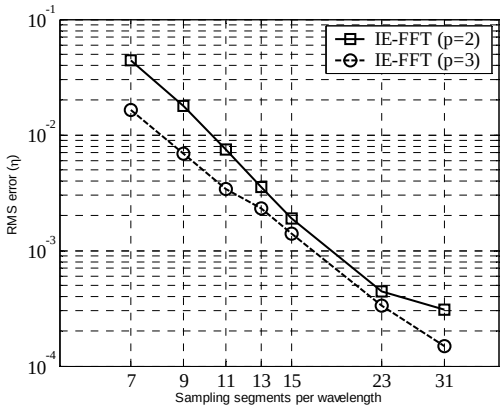

Fig. 6 The RMS error of bistatic SCS calculation versus sampling segments per wavelength. A 4λ PEC sphere is tested and the RMS error is relative to that of MoM solution. The second-order and third-order Lagrange polynomials are used.

B. Generic battleship

A realistic example considered here is a generic battleship. When the plane wave is incident from the nose direction, the bistatic SCS of $\theta\theta$ -polarization is computed by the IE-FFT algorithm and conventional MoM. Fig.9 shows the comparison between the bistatic SCS from the IE-FFT algorithm and the result of the conventional MoM at 30MHz. Both results agree very well.

In the next experiment, the frequency of operation is increased to 60MHz. The results of the IE-FFT algorithm are compared with those of ACA algorithm [9], as shown in Fig.10. The result of IE-FFT algorithm agrees well with that of ACA algorithms. Finally, the bistatic scattering of the battleship at the frequency of 240 MHz is considered in Fig. 11. In the IE-FFT computations N = 739,416 unknowns (corresponds to an average discretization size of $h = \lambda/5$) are involved along with a third-order Green's function interpolation. The memory of MoM and Π matrices, and the coefficients of Green's function are about 4.3 GB. Two polar plots are also shown in Fig. 11. The left and right figures are plots in the azimuth and elevation planes, respectively. The bistatic SCS of $\phi\phi$-polarization is plotted in Fig. 12.

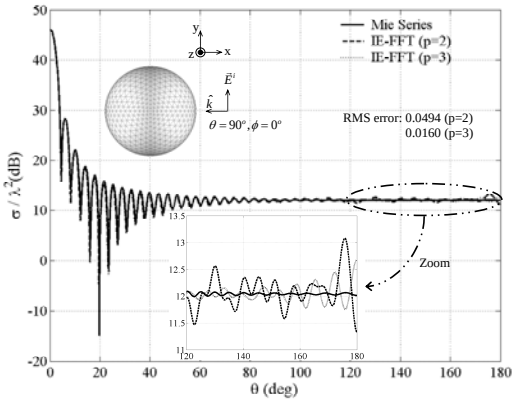

Fig. 7 Bistatic SCS for a PEC 16λ sphere. The results of the IE-FFT algorithm are compared with those of Mie series. It corresponds to 196,608 RWG unknowns.

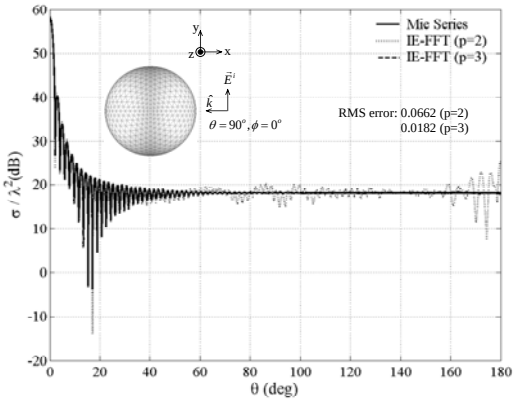

Fig. 8 Bistatic SCS for a PEC 32λ sphere. The results of the IE-FFT algorithm are compared with those of Mie series. It corresponds to 786,432 RWG unknowns.

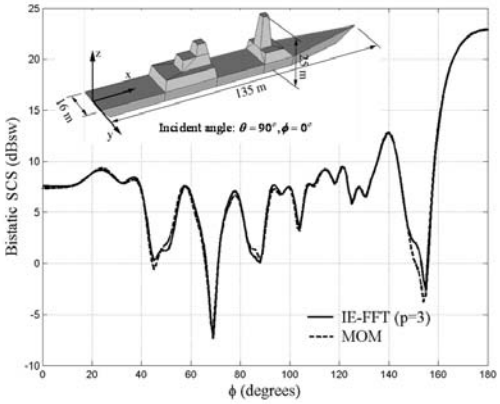

Fig. 9 Comparisons of the bistatic SCS for the battleship at 30 MHz ($\theta\theta$-polarization) using the IE-FFT and the conventional MoM.

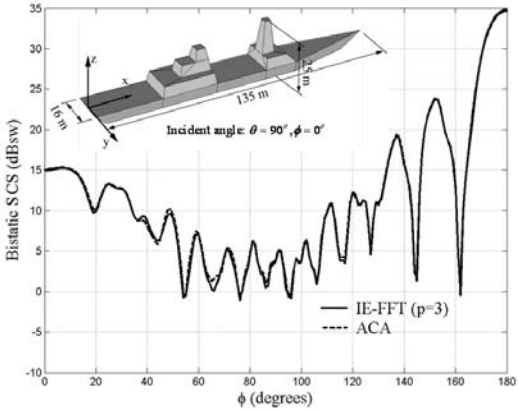

Fig. 10 Comparisons of the bistatic SCS for the battleship at 60 MHz ($\theta\theta$ -polarization) using the IE-FFT and the ACA algorithm [9].

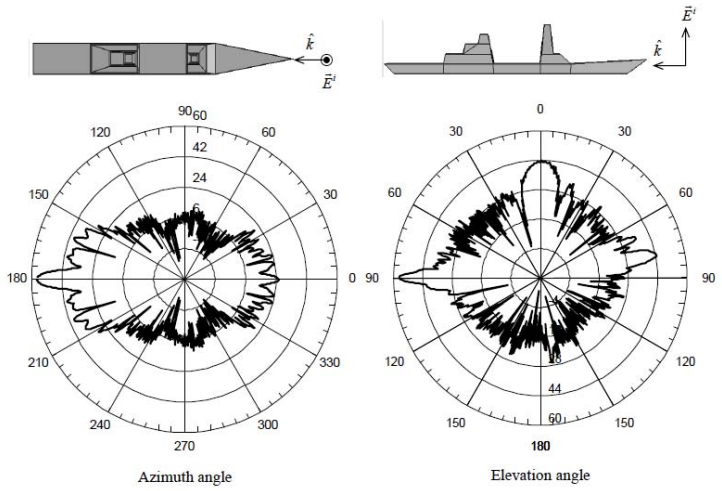

Fig. 11 The computed bistatic SCS of the battle ship at 240 MHz ($\theta\theta$ -polarization) using the IEFFT.

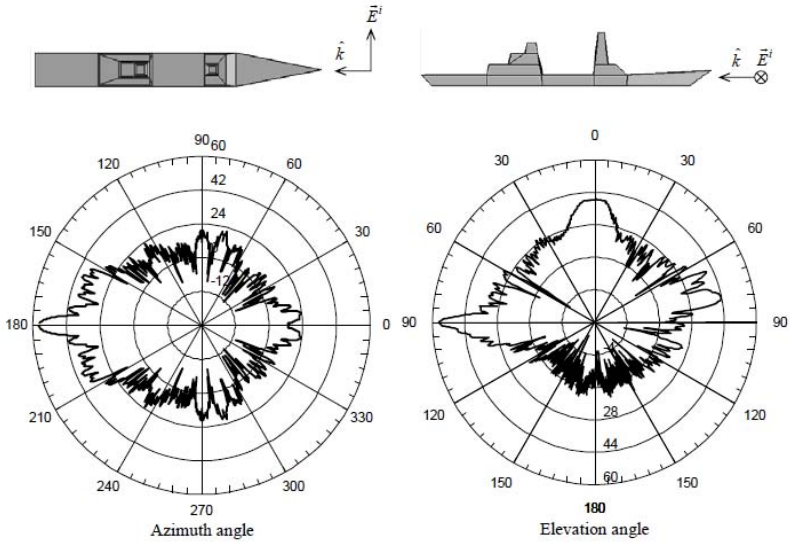

Fig. 12 The computed bistatic SCS of the battle ship at 240 MHz ($\phi\phi$ –polarization) using the IEFFT.

REFERENCES

[1] V. Rokhlin, "Rapid Solution of Integral Equations of Classical Potential Theory," *J. Comput. Phy.*, vol. 60, pp. 187-207, 1985.

[2] J. M. Song and W. C. Chew, "Multilevel Fast Multipole Algorithm for Solving Combined Field Integral Equation of Electromagnetic Scattering," *Mico. Opt. Tech. Lett.*, vol. 10, no. 1, pp. 14-19, Sep. 1995.

[3] R. Coifman, V. Rokhlin, and S. Wandzura, "The Fast Multipole Method for the Wave Equation: A Pedestrian Prescription," *IEEE Antennas Propagat. Mag.*, vol. 35, no. 3, pp. 7-12, Jun 1993.

[4] B. Dembart and E. Yip, "The Accuracy of Fast Multipole Methods for Maxwell's Equations," *IEEE Comput. Sci. Eng.*, vol. 5, no.3, 48-56, 1998.

[5] J. S. Zhao and W. C. Chew, "Three-dimensional Multilevel Fast Multipole Algorithm from Static to Electrodynamic," *Micro. Opt. Tech. Lett.*, vol. 26, no. 1, pp. 43-48, July 2000.

[6] S. Kapur and D. E. Long, "IES3: A Fast Integral Equation Solver for Efficient 3-Dimensional Extraction," *In 37th International Conference on Computer Aided Design*, Nov. 1997.

[7] S. M. Seo and J. F. Lee, "A Single-Level Low Rank IE-QR Algorithm for PEC Scattering Problems Using EFIE Formulation," *IEEE Trans. Antenna Propagat.*, vol. 52, no. 8, pp. 2141-2146, Aug. 2004.

[8] K. Zhao and J. F. Lee, "A Single-Level Dual Rank IE-QR Algorithm to Model Large Microstrip Antenna Arrays," *IEEE Trans. Antennas Propagat.*, vol. 52, no.10, pp. 2580-2585, Oct 2004.

[9] K. Zhao, M. N. Vouvakis, and J. F Lee, "Application of the Multilevel Adaptive Cross-Approximation on Ground Plane Designs," *IEEE EMC Symposium*, Santa Clara, CA, Aug. 9-13, 2004.

[10] S. Kurz, O. Rain, and S. Rjasanow, "The Adaptive Cross-Approximation Technique for the 3-D Boundary Element Method," *IEEE Tans. Magn.*, vol. 38, pp. 421-424, Mar. 2002.

[11] J. R. Phillips and J. K. White, "A Precorrected-FFT Method for Electrostatic Analysis of Complicated 3-D Structures," *IEEE Trans. Computed-Aided Design of Integrated Circuits and Systems*, vol. 16, pp. 1059-1072, 1997.

[12] J. R. Phillips, "Error and Complexity Analysis for A Collocation-Grid-Projection Plus Precorrected-FFT Algorithm for Solving Potential Integral Equations with Laplace or Helmholtz Kernels," in *Proc. 1995 Copper Mountain Conf. Multigrid Methods*, Apr. 1995.

[13] E. Bleszynski, M. Bleszynski, and T. Jaroszewicz, "AIM: Adaptive Integral Method for Solving Large-scale Electromagnetic Scattering and Radiation Problems," *Radio Science*, vol. 31, no. 5, pp. 1225-1251, 1996.

[14] C. F. Wang, F. Ling, J. M. Jin, "Adaptive Integral Solution of Combined Field Integral Equation," *Microwave Opt. Tech. Lett.*, vol. 19, no 5, pp. 321-328, Dec. 1998.

[15] O. P. Bruno and L. A. Kunyansky, "A Fast, High-Order Algorithm for the Solution of Surface Scattering Problems: Basic Implementation, Tests, and Applications," *J. Comput. Phy.*, 169, 80-110, 2001.

[16] S. Q. Li, Y. Yu, C. H. Chan, K. F. Chan, and L. Tsang, "A Sparse-Matrix/Canonical Grid Method for Analyzing Densely Packed Interconnects," *IEEE Trans. Micro. Theory Tech.*, vol. 49, no. 7, pp. 1221-1228, July 2001.

[17] S. Gedney, A. Zhu, W. H. Tang, G. Liu, and P. Petre, "A Fast, High-order Quadrature Sampled Pre-corrected Fast-Fourier Transform for Electromagnetic Scattering," *Microwave Opt. Tech. Lett.*, vol. 36, no. 5, Mar. 5 2003.

[18] B. J. Fasenfest, F. Capolino, D. R. Wilton, D. R. Jackson, and N. J. Champagne, "A Fast MoM Solution for Large Arrays: Green's Function Interpolation with FFT," *IEEE Antennas Wireless Propagat. Lett.*, vol. 3, pp. 161-164, 2004.

[19] S. M. Rao, D. R. Wilton, and A. W. Glisson, "Electromagnetic Scattering by Surfaces of Arbitrary Shape," *IEEE Trans. Antennas Propagat.*, vol. AP-30, pp. 409-418, May 1982.

[20] M. N. Vouvakis, S.-C. Lee, K. Zhao, and J.-F. Lee, "A Symmetric FEM-IE Formulation with a Single-Level IE-QR Algorithm for Solving Electromagnetic Radiation and Scattering Problems," *IEEE Trans. Antennas Propagat.*, vol. AP-52, pp. 409-418, Nov. 2004.

[21] P. J. Davis, *Interpolation & Approximation*, pp. 56, Dover publication, New York.

[22] W. C. Chew, "Computational Electromagnetics: The Physics of Smooth Versus Oscillatory Fields," *Phil. Trans. R. Soc. Lond. A*, vol. 362, pp. 579-602, 2004.

Chao-Fu Wang received the B.Sc. degree in mathematics from the Henan Normal University, China, in 1985, the M.Sc. degree in applied mathematics from the Hunan University, China, in 1989, and the Ph.D. degree in electrical engineering from the University of Electronic Science and Technology of China in 1995. From 1987 to 1996, he was a Lecturer, and then an Associate Professor at the

Nanjing University of Science and Technology, China. From 1996 to 1999, he was a Postdoctoral Research Fellow in the Center for Computational Electromagnetics, University of Illinois at Urbana-Champaign. From 1999 to 2001, he was a Research Fellow in the Department of Electrical and Computer Engineering, National University of Singapore (NUS), Singapore. He was transferred to Temasek Laboratories at NUS as a Research Scientist in 2001, where he currently is a Senior Research Scientist and Head of Propagation & Scattering Group. His research interests include fast algorithms for computational electromagnetics, scattering and antenna analysis, ferrite components and their analysis, MMIC design and fast EM simulation.

Jin-Fa Lee received the B.S. degree from National Taiwan University, in 1982 and the M.S. and Ph.D. degrees from Carnegie-Mellon University in 1986 and 1989, respectively, all in electrical engineering. From 1988 to 1990, he was with ANSOFT Corp., where he developed several CAD/CAE finite element programs for modeling three-dimensional microwave and millimeter-wave circuits. From 1990 to 1991, he was a post-doctoral fellow at the University of Illinois at Urbana-Champaign. From 1991 to 2000, he was with Department of Electrical and Computer Engineering, Worcester Polytechnic Institute. Currently, he is a Professor at ElectroScience Lab., Dept. of Electrical Engineering, Ohio State University. Prof. Lee becomes an IEEE Fellow on year 2005. His students won the 4th place in student paper contest in IEEE APS/URSI 2004, 3rd place in IEEE APS/URSI 2005, and 1st place in EMC Zurich 2006, and were the two finalists in the APS/URSI 2006 student paper contest. Professor Lee's research interests mainly focus on numerical methods and their applications to computational electromagnetics. Current research projects include: analyses of numerical methods, fast finite element methods, fast integral equation methods, three-dimensional mesh generation, domain decomposition methods, hybrid numerical methods and high frequency techniques based on domain decompositions approach, and RFID tag antenna designs, and large antenna arrays and Rotman lens.